

Lithium-Metal Batteries

International Edition: DOI: 10.1002/anie.201702099

German Edition: DOI: 10.1002/ange.201702099

Lithiophilic Sites in Doped Graphene Guide Uniform Lithium Nucleation for Dendrite-Free Lithium Metal Anodes

Rui Zhang⁺, Xiao-Ru Chen⁺, Xiang Chen⁺, Xin-Bing Cheng⁺, Xue-Qiang Zhang, Chong Yan, and Qiang Zhang*

Abstract: Lithium (Li) metal is the most promising electrode for next-generation rechargeable batteries. However, the challenges induced by Li dendrites on a working Li metal anode hinder the practical applications of Li metal batteries. Herein, nitrogen (N) doped graphene was adopted as the Li plating matrix to regulate Li metal nucleation and suppress dendrite growth. The N-containing functional groups, such as pyridinic and pyrrolic nitrogen in the N-doped graphene, are lithiophilic, which guide the metallic Li nucleation causing the metal to distribute uniformly on the anode surface. As a result, the N-doped graphene modified Li metal anode exhibits a dendrite-free morphology during repeated Li plating and demonstrates a high Coulombic efficiency of 98 % for near 200 cycles.

With the booming advances in high-end electronic devices, high-energy-density batteries are needed to alleviate concerns about battery endurance.^[1,2] Since the Li metal anode possesses an ultrahigh theoretical specific capacity (3860 mA h g⁻¹) and the lowest negative electrochemical potential (-3.040 V vs. the standard hydrogen electrode), Li metal batteries (LMBs) are therefore recognized as one of the most promising candidates.^[1] However, the formation of Li dendrites during repeated Li plating/stripping cycles will not only induce many “dead Li” with capacity loss, but also have the potential to cause internal short circuit and other hazardous issues.^[1,3] Therefore, Li dendrites and their related issues severely hinder the practical applications of LMBs.

To address these issues, significant progress has been achieved recently, in areas including liquid electrolyte modifications,^[4] artificial electrode/electrolyte films,^[5] solid-state^[6] or polymer^[7] electrolytes, hybrid electrolytes,^[8] and nanostructured anodes with high surface areas.^[9] However, these result-oriented approaches mainly concentrate on the already obtained Li plating morphology induced by existing methods, but less involve the initial nucleation process. Actually, the final morphology critically depends on the initial nucleating behavior. Systematic investigation of Li metal nucleation

behavior is of great significance. Suppressing Li dendrite growth at the nucleating stages is expected to lead to a safe and efficient LMB and offer a mechanistic understanding of the working Li metal battery as well.

Very recently, Cui and co-workers^[10] have conducted experimental work to consider the initial nucleation stage of Li deposition. The Li nuclei size is heavily dependent on the current density, confirming the effectiveness of reducing the local current density by introducing a high-surface-area Li plating matrix.^[10] More importantly, the nucleation sites greatly rely on the type of Li plating matrix and a “lithiophilic” matrix is preferred for Li metal nucleation with a reduced polarization. A “lithiophilic” matrix that has a good metallic Li affinity can be wet by molten Li, which indicates a strong binding energy between Li atoms and the surface of the matrix. Therefore, designing a Li plating matrix with a high surface area and lithiophilic surface makes much sense for a safe and efficient Li metal anode.

Herein we report a nitrogen-doped graphene (NG) matrix with densely and uniformly distributed lithiophilic functional groups designed to guide Li metal nucleation and growth. The NG can inhibit Li dendrite growth by regulating Li nucleation sites and sizes. The electrochemical performance of NG-based Li metal anodes was therefore improved with dendrite-free Li deposits in a working battery.

The nucleation and plating processes of metallic Li on NG-based and Cu foil-based current collector are schematically illustrated in Figure 1. Li ions start to migrate toward anode surface under the dual effect of the electric field and concentration gradient at the beginning of Li plating. The Li ions that reach the current-collector surface will acquire electrons and start nucleation. When employing Cu foil (a general control sample in the research of Li metal anodes) as

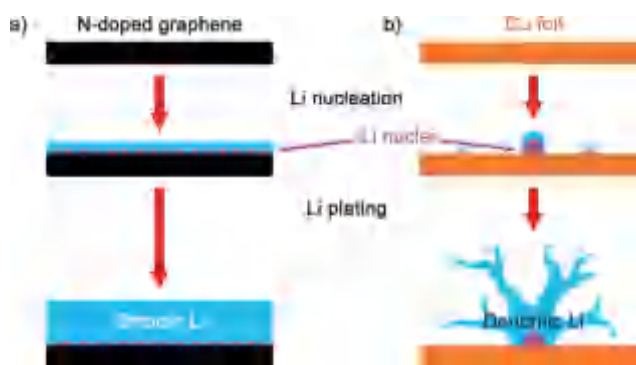


Figure 1. Schematic representation of the Li nucleation and plating process on a) N-doped graphene electrode and b) Cu foil electrode.

[*] R. Zhang,^[†] X.-R. Chen,^[†] X. Chen,^[†] X.-B. Cheng,^[†] X.-Q. Zhang, C. Yan, Prof. Q. Zhang
Beijing Key Laboratory of Green Chemical Reaction Engineering and Technology, Department of Chemical Engineering
Tsinghua University
Beijing 100084 (P.R. China)
E-mail: zhang-qiang@mails.tsinghua.edu.cn

[†] These authors contributed equally to this work.

Supporting information and the ORCID identification number(s) for the author(s) of this article can be found under:
<https://doi.org/10.1002/anie.201702099>.

the current collector, the nucleation sites for Li plating are isolated and randomly distributed owing to the heterogeneous and rough surface of the Cu foil, which tends to induce a non-uniform Li deposition. Since the Cu foil is not lithiophilic, the overpotential for metallic Li plating on the Cu foil surface is much higher than that on a Li-metal surface. Thus on Cu, Li atoms are more likely to continuously deposit on existed Li nucleation deposits, hence resulting in a dendritic morphology.^[10] In the following growth stage, Li nucleation deposits mainly grow in the direction away from the surface and eventually form large Li dendrites, controlled by the combined effect of the electric field and the concentration gradient.^[11] When employing a N-doped graphene framework as the Li plating matrix, both the plating process and final morphology are significantly improved. The surface of N-doped graphene is full of lithiophilic functional groups, such as pyridinic, pyrrolic, and quaternary nitrogen atoms, offering much more uniform nucleation sites and a smaller nucleation overpotential than the Cu foil surface. Therefore, metallic Li deposits preferentially on the N-doped graphene surface. When complete, the surface of the NG will be covered with uniform and smooth Li deposits.

The NG employed herein was synthesized by treating graphene in ammonia under 600 °C for 4 h.^[12] The as-obtained NG has a nitrogen content of 3.14 atom % as determined by X-ray photoelectron spectroscopy (XPS). The fitting result of the N 1s fine scan spectra exhibits three peaks (Figure 2a), assigned to pyridinic nitrogen (pnN, 398.5 eV), pyrrolic nitrogen (prN, 400.2 eV), and quaternary nitrogen (qnN, 402.1 eV). Quaternary nitrogen in the bulk phase (qnN) was not obtained according to XPS (Figure 2b). Both pyridinic and pyrrolic nitrogen are the two main components among these N-containing functional groups in these NG scaffolds.

To probe the metallic-Li deposition process and the interactions between the Li atom and Cu or different functional groups, binding energy and charge density analyses were conducted based on density functional theory (DFT) calculations (Figure 2c). There is only a weak interaction between Li atom and Cu slab (Figure 2d and Figure S1 in the Supporting Information). In contrast, the edge and high-coordination sites in graphene and NG with functional groups are preferred for Li atoms adsorption (Figure S2, Supporting Information). Pyrrolic nitrogen and pyridinic nitrogen exhibit relatively larger binding energies of -4.46 and -4.26 eV than graphene of -3.64 eV and Cu of -2.57 eV. The local charge density between pyrrolic nitrogen and Li atom is increased (Figure 2e,f), indicating the strong interaction between Li and N atoms. Note that there is one extra electron in the pyrrolic nitrogen group, in which N provides a pair of p-electrons to conjugated π bond, while there are lone-pair electrons in the pyridinic nitrogen. The NG nanosheets with extra pair of electrons are expected as electron-rich donors with filled p orbitals that naturally act as Lewis base sites to strongly adsorb Lewis acidic Li ions in electrolytes through acid–base interactions, guiding the metallic Li nuclei to uniformly distribute on the anode surface.^[13] However, the quaternary nitrogen (both qN and qnN) with saturated electron orbitals is not able to afford extra lone-pair electrons for adsorbing Li atoms, resulting in a relatively weak binding energy (Fig-

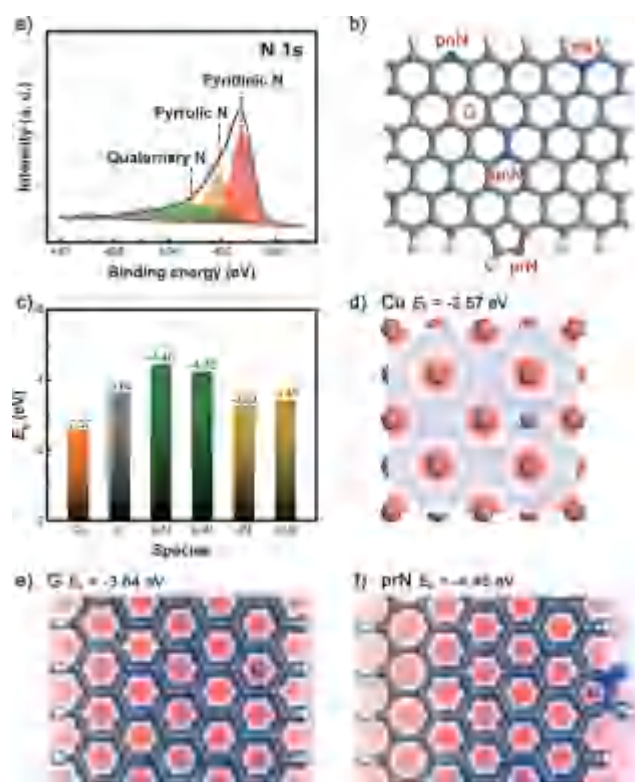


Figure 2. N species and their binding with Li. a) N 1s XPS spectra of N-doped graphene. b) Schematic diagram of N-doped graphene with pyridinic nitrogen (pnN), pyrrolic nitrogen (prN), quaternary nitrogen on the edge (qN) and quaternary nitrogen in the bulk phase (qnN). c) Binding energy of a Li atom with Cu, graphene (G), and different functional groups of N-doped graphene. The deformation charge density at a Li atom adsorption site of: d) Cu, e) graphene, and f) pyrrolic-N group. An increase in total electron density with the density of isolated atoms subtracted is shown as blue, a decrease as red.

ure 2c). The main nitrogen-containing functional groups of the NG employed are pyridinic nitrogen and pyrrolic nitrogen, thus, the surface of NG can have a strong interaction with Li atoms. A stronger binding energy of Li atoms can always lead to a better adsorption of Li ions (Figure S3). Therefore, Li ions are expected to adsorb and plate as metallic Li atoms on the lithiophilic sites related to these nitrogen-containing functional groups. In addition, according to our calculations the doped N atoms cannot react with plated Li atoms to form Li_3N (Figure S2, Supporting Information), which means that the doped N atoms possess electrochemical stability in LMBs.

To directly demonstrate the lithiophilicity of such NG materials, surface wetting experiments of molten Li on Cu, graphene, and NG have been conducted (Figure S4). For NG material, the molten Li can wet and spread onto the NG surface giving a smaller contact angle than that on Cu and graphene surface.

Furthermore, nucleation overpotentials are employed to evaluate the degree of lithiophilicity on the electrode surface quantitatively. There is a certain overpotential between the two electrodes in the galvanostatic electrochemical deposition of metallic Li. A part of this overpotential is induced by

the mass-transfer resistance, which is present throughout the whole metal-Li deposition process. The mass-transfer overpotential is mainly affected by the current density and the migration properties of Li ions in electrolyte. The other part is the nucleation overpotential, which exists only in the short nucleation stage at the beginning of deposition. The nucleation overpotential is necessary for metallic Li to deposit on the surface of the heterogeneous electrode. The nucleation overpotential mainly depends on the lithiophilicity of the electrode surface. Some metals, such as Au and Ag, that form an alloy with Li metal can provide a zero nucleation potential.^[14]

The overpotentials of metallic Li plating on Cu foil and NG electrodes induced by different binding strengths were investigated (Figure 3a). A sharp voltage drops to -0.062 V (vs. Li/Li^+) is recorded at the beginning of the Li plating process on Cu foil electrode, which relates to the nucleation process of metallic Li. After nucleation, the voltage rises to a relatively stable voltage platform at -0.009 V, which is the mass-transfer-controlled overpotential. The nucleation overpotential μ_n is defined as the difference between the sharp tip voltage and the later stable mass-transfer-controlled overpotential, which is 0.053 V for Cu foil electrode. In contrast, the curve of NG electrode exhibits much more smooth voltage dip at the nucleation stage, with a nucleation overpotential of only 0.022 V, which is much smaller than that of Cu foil electrode. Owing to the lithiophilic nitrogen containing functional groups in N-doped graphene, the NG electrode exhibits lower resistance for metallic Li to plate at the electrode surface, instead of plating on Li deposits to form long dendrites.

Of note is that the specific surface area of NG is 380.7 m^2g^{-1} (Figure S5), which significantly reduces the local current density to minimize the overpotential. To exclude the effect of the high-surface-area of the scaffolds on Li nucleation in the NG, the nucleation overpotential of graphene (G, the raw materials for NG, with a similar specific surface area of 380.2 m^2g^{-1}) is measured to be 0.029 V at the same current density of 0.05 mA cm^{-2} . This nucleation overpotential is between these of Cu foil and NG electrodes, demonstrating that the introduction of nitrogen-containing functional groups indeed facilitates the Li nuclei formation on NG electrodes, not merely contributed by the high specific surface area. Since the nitrogen-containing functional groups endow NG with the lithiophilic surface, the N content directly affects the lithiophilicity of NG. The surface of NG becomes more lithiophilic with the higher N content, which brings a lower nucleation overpotential. However, a too high N content may destroy the conjugate structure of graphene and then reduce the electrical conductivity, which is not beneficial to Li deposition.

The nucleation potentials at different current densities ranging from 0.01 to 1.0 mA cm^{-2} were also investigated (Figure 3b and Figure S6). The μ_n on NG electrode increases from 0.017 to 0.036 V with the increase in current density, which is much slower than that on Cu foil electrode from 0.020 to 0.103 V. The NG electrode can also effectively

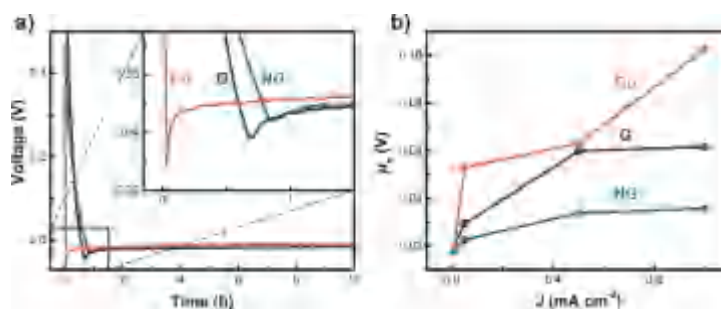


Figure 3. Nucleation overpotential. a) The voltage–time curves during Li nucleation at 0.05 mA cm^{-2} on Cu foil, G, and NG electrodes. b) The Li nucleation overpotentials (μ_n) on Cu, G, and NG electrodes at different current densities (j).

regulate the metallic Li nucleation on electrode surface at higher current densities.

Li nucleating and plating process induced by the N-containing groups on NG were further illustrated by SEM characterization (Figure 4). The metallic Li was plated at a current density of 0.05 mA cm^{-2} with a nucleation capacity of 0.25 mA h cm^{-2} (5 h). The fully plated Li morphology was obtained on NG electrode (Figure 4c), indicating the successful control of Li plating at the nucleation stage. In contrast, the scattered large Li nucleation deposits were clearly observed on Cu foil electrode (Figure 4d). Some

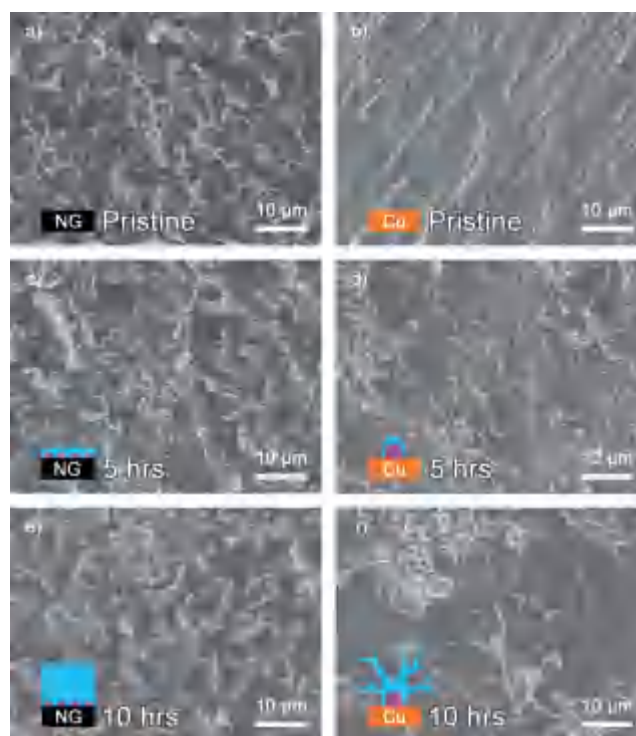


Figure 4. SEM images of metallic Li deposits at a low current density of 0.05 mA cm^{-2} . The morphology of pristine a) NG electrode and b) Cu foil electrode. The morphology of Li nuclei on c) NG electrode and d) Cu foil electrode with the nucleation capacity of 0.25 mAh cm^{-2} . The morphology of e) NG electrode and f) Cu foil electrode with the plated Li of 0.50 mAh cm^{-2} . Insets in bottom left corners schematically show the growth phase.

nucleation deposits have finally grown into Li dendrites with a length of few micrometers.

To further compare the Li deposit morphology after the nucleation stage, a continuous Li plating was conducted with a total plating capacity of $0.50 \text{ mA h cm}^{-2}$ (10 h) (Figure 4e,f). A filling in the slit pores of NG and an increase in the thickness of NG flakes are observed, indicating the smooth morphology of the Li deposits without Li dendrites (Figure 4e). However, the deposits on Cu foil electrode are full of Li dendrites with the length more than tens of micrometers (Figure 4f). The dendrite growth on Cu foil electrode and the dendrite-free morphology on NG electrode are also verified in another plating process at a higher current density of 0.50 mA cm^{-2} with a higher plating capacity of 2.0 mA h cm^{-2} (4 h, Figure S7), indicating that the dendrite growth on Cu foil is almost not influenced by the current density. The nucleation guidance from the nitrogen containing functional groups on NG plays a critical role in the dendrite-free morphology.

The electrochemical performance in a working Li metal battery is a critical indicator for the application prospects of such NG based Li metal anodes with dendrite-free morphology. The two electrode cells were assembled to probe the cycling performance. Coulombic efficiency defined as the ratio of Li stripping capacity to Li plating capacity at each cycle is a frequently adopted index to evaluate the electrochemical performance of Li metal anodes. The Coulombic efficiency of NG electrode at 1.0 mA cm^{-2} with a cycling capacity of 1.0 mA h cm^{-2} maintains 98% for near 200 cycles, while that of Cu foil electrode oscillates around 90% and decreases below 70% in 70 cycles (Figure 5a). When the cycling capacity is increased to 2.0 mA h cm^{-2} , the Coulombic

efficiency of NG electrode still reach 98% for more than 50 cycles, which was much more stable and higher than that of Cu foil electrode (Figure 5b) or other nanostructured composite anode.^[15] The high pore volume of $1.93 \text{ cm}^3 \text{ g}^{-1}$ (Figure S5) guarantees the NG electrode with a stable high capacity cycling performance. Therefore, the Coulombic efficiency of NG electrode keeps around 97% at an even higher cycling capacity of 5.0 mA h cm^{-2} (Figure S8). When conducted at a higher current density of 2.0 mA cm^{-2} , the Coulombic efficiency on NG electrode still reached 96% for 100 cycles (Figure S8). The capacity loss during cycles has been effectively inhibited without dendrite growth. Therefore, NG electrode affords a very stable and high Coulombic efficiency to Li metal batteries with NG based anodes.

The Li plating/stripping behaviors on Cu foil and NG electrode are probed by the charge–discharge curves (Figure 5c). The discharging voltage profiles of Cu foil are clearly shorter in the time scale than the charging ones, indicating the large amount of irreversible capacity loss. However, the capacity loss on NG electrode is inconspicuous due to the high Coulombic efficiency of 98%. The hysteresis in the voltage profile is only 0.05 V for NG electrode, much smaller than that for Cu foil electrode (0.07–0.12 V). An extremely lower interface impedance of NG electrode than the one of Cu foil electrode after the 50th plating process has also been verified by impedance spectroscopy (Figure S9). These advantages are introduced by the low local current density that decreases the areal mass transfer resistance and the lithiophilic functional groups binding plated Li atoms with the 3D graphene framework.

The long-cycle stability of NG electrode was investigated with a systematic Li | Li test. The working Cu foil and NG electrodes were firstly plated by Li metal with a pre-stored capacity of 4.0 mA h cm^{-2} , then cycled at a current density of 1.0 mA cm^{-2} and a cycling capacity of $0.042 \text{ mA h cm}^{-2}$ (Figure 5d). NG electrode showed a much more stable cycling than Cu foil electrode, indicating the stable plating and stripping process with the NG electrode in a working battery.

In addition to the benefits from the lithiophilic N containing functional groups, the reduced local current density induced by the relatively high specific surface area of NG ($380.7 \text{ m}^2 \text{ g}^{-1}$) has also contributed to the dendrite-free morphology and the excellent electrochemical performance. Such medium-sized surface area can avoid the vast consumption of active materials in extensive SEI formation. Besides, the smooth surface of NG can also homogenize the charge distribution and avoid the dendrites caused by electronic effects.

The NG based Li metal anode exhibits impressive performance in both Li dendrite inhibition and electrochemical performance. All these improvements mainly benefit from the effective regulation on Li nucleation and the following growth processes. Metallic Li can be plated uniformly on the surface of NG electrode, rather than on the pre-formed Li deposits on Cu foil to form Li dendrites, due to the lithiophilic nature of NG. With the calculation on the binding

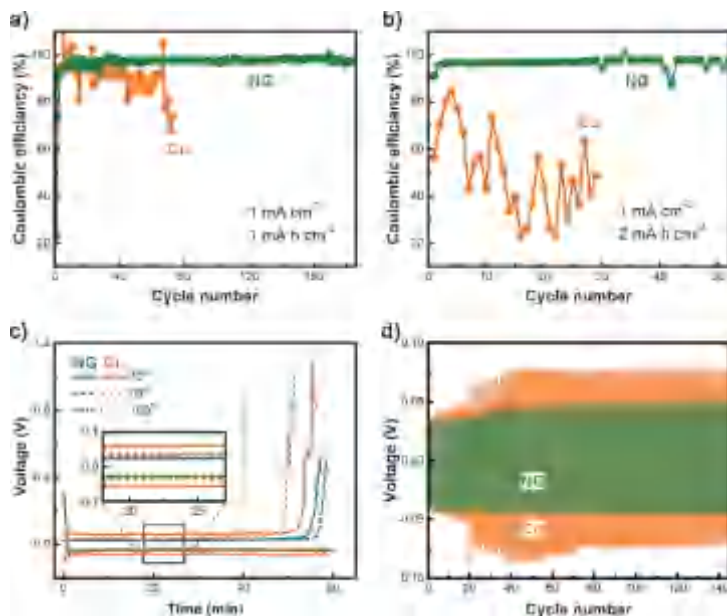


Figure 5. Electrochemical performance. Coulombic efficiency of Cu foil and NG electrode with a cycling capacity of a) 1.0 mA h cm^{-2} , b) 2.0 mA h cm^{-2} at the same current density of 1.0 mA cm^{-2} . c) Voltage profiles of the 10th, 50th, and 100th cycle of Cu foil and NG electrode with a cycling capacity of 1.0 mA h cm^{-2} at 1.0 mA cm^{-2} . d) Voltage–time curves in 150 cycles of Cu foil and NG electrode at a cycling current density at 1.0 mA cm^{-2} .

energy of Li atom with Cu foil and N-doped graphene, we consider that some of the nitrogen containing functional groups like pyridinic nitrogen and pyrrolic nitrogen play the key role in making N-doped graphene a lithiophilic matrix, which can lead Li ions to adsorb and Li atoms to deposit uniformly on the electrode surface.

In summary, we have performed proof-of-concept investigations on a novel matrix containing uniform lithiophilic sites to regulate metallic Li nucleation and suppress Li dendrite growth. With the lithiophilic nitrogen-containing functional groups, such as pyridinic nitrogen and pyrrolic nitrogen, the N-doped graphene can regulate the nucleation process of metallic Li electrodeposition. As a result, dendrite-free Li metal deposits were obtained, which make the N-doped graphene electrodes exhibit an impressive electrochemical performance. The Coulombic efficiency of the N-doped graphene electrode at a current density of 1.0 mA cm^{-2} and a cycle capacity of 1.0 mAh cm^{-2} can be maintained at 98% for nearly 200 cycles. The strategy emphasizes the importance of Li nucleation on the Li plating morphology, which can suppress Li-dendrite growth at a sprouting stage. The prospects presented herein can shed a new light on Li metal deposition and are instructional to other metal batteries as well.

Acknowledgements

This work was supported by National Key Research and Development Program (Nos. 2016YFA0202500 and 2016YFA0200102), Natural Scientific Foundation of China (Nos. 21422604, 21676160, and 21276141), Tsinghua University Initiative Scientific Research Program, and Tsinghua National Laboratory for Information Science and Technology. We thank Chen-Zi Zhao, Hong-Jie Peng, and Prof. Jia-Qi Huang for helpful discussion.

Conflict of interest

The authors declare no conflict of interest.

Keywords: lithium dendrites · lithium metal anode · nitrogen-doped graphene · nucleation and growth · rechargeable batteries

How to cite: *Angew. Chem. Int. Ed.* **2017**, *56*, 7764–7768
Angew. Chem. **2017**, *129*, 7872–7876

- [1] W. Xu, J. L. Wang, F. Ding, X. L. Chen, E. Nasybutin, Y. H. Zhang, J. G. Zhang, *Energy Environ. Sci.* **2014**, *7*, 513–537.
- [2] Y. Sun, N. Liu, Y. Cui, *Nat. Energy* **2016**, *1*, 16071; X.-B. Cheng, R. Zhang, C.-Z. Zhao, F. Wei, J.-G. Zhang, Q. Zhang, *Adv. Sci.* **2016**, *3*, 1500213; K. Zhang, G. H. Lee, M. Park, W. J. Li, Y. M. Kang, *Adv. Energy Mater.* **2016**, *6*, 1600811.
- [3] D. Aurbach, E. Zinigrad, H. Teller, P. Dan, *J. Electrochem. Soc.* **2000**, *147*, 1274–1279.
- [4] R. R. Miao, J. Yang, X. J. Feng, H. Jia, J. L. Wang, Y. N. Nuli, *J. Power Sources* **2014**, *271*, 291–297; J. Qian, W. A. Henderson, W. Xu, P. Bhattacharya, M. Engelhard, O. Borodin, J.-G. Zhang,

- Nat. Commun.* **2015**, *6*, 6362; L. Suo, Y.-S. Hu, H. Li, M. Armand, L. Chen, *Nat. Commun.* **2013**, *4*, 1481; W. Li, H. Yao, K. Yan, G. Zheng, Z. Liang, Y.-M. Chiang, Y. Cui, *Nat. Commun.* **2015**, *6*, 7436; X.-Q. Zhang, X.-B. Cheng, X. Chen, C. Yan, Q. Zhang, *Adv. Funct. Mater.* **2017**, *27*, 1605989.
- [5] Y. Liu, D. Lin, P. Y. Yuen, K. Liu, J. Xie, R. H. Dauskardt, Y. Cui, *Adv. Mater.* **2017**, *29*, 1605531; G. Y. Zheng, S. W. Lee, Z. Liang, H. W. Lee, K. Yan, H. B. Yao, H. T. Wang, W. Y. Li, S. Chu, Y. Cui, *Nat. Nanotechnol.* **2014**, *9*, 618–623; N. W. Li, Y. X. Yin, C. P. Yang, Y. G. Guo, *Adv. Mater.* **2016**, *28*, 1853–1858; X.-B. Cheng, C. Yan, X. Chen, C. Guan, J.-Q. Huang, H.-J. Peng, R. Zhang, S.-T. Yang, Q. Zhang, *Chem* **2017**, *2*, 258–270; Q. C. Liu, J. J. Xu, S. Yuan, Z. W. Chang, D. Xu, Y. B. Yin, L. Li, H. X. Zhong, Y. S. Jiang, J. M. Yan, X. B. Zhang, *Adv. Mater.* **2015**, *27*, 5241–5247; M. H. Ryou, Y. M. Lee, Y. J. Lee, M. Winter, P. Bieker, *Adv. Funct. Mater.* **2015**, *25*, 834–841.
- [6] Z. Tu, Y. Lu, L. Archer, *Small* **2015**, *11*, 2631–2635; Y. Lu, M. Tikekar, R. Mohanty, K. Hendrickson, L. Ma, L. A. Archer, *Adv. Energy Mater.* **2015**, *5*, 1402073; Q. W. Pan, D. M. Smith, H. Qi, S. J. Wang, C. Y. Li, *Adv. Mater.* **2015**, *27*, 5995–6001; D. Zhou, R. Liu, Y.-B. He, F. Li, M. Liu, B. Li, Q.-H. Yang, Q. Cai, F. Kang, *Adv. Energy Mater.* **2016**, *6*, 1502214; X. Y. Yao, D. Liu, C. S. Wang, P. Long, G. Peng, Y. S. Hu, H. Li, L. Q. Chen, X. X. Xu, *Nano Lett.* **2016**, *16*, 7148–7154; X. Han, Y. Gong, K. Fu, X. He, G. T. Hitz, J. Dai, A. Pearse, B. Liu, H. Wang, G. Rubloff, Y. Mo, V. Thangadurai, E. D. Wachsman, L. Hu, *Nat. Mater.* **2017**, *16*, 572–579.
- [7] D. C. Lin, D. Zhuo, Y. Y. Liu, Y. Cui, *J. Am. Chem. Soc.* **2016**, *138*, 11044–11050; X. X. Zeng, Y. X. Yin, N. W. Li, W. C. Du, Y. G. Guo, L. J. Wan, *J. Am. Chem. Soc.* **2016**, *138*, 15825–15828.
- [8] Y. Y. Lu, K. Korf, Y. Kambe, Z. Y. Tu, L. A. Archer, *Angew. Chem. Int. Ed.* **2014**, *53*, 488–492; *Angew. Chem.* **2014**, *126*, 498–502; W. D. Zhou, S. F. Wang, Y. T. Li, S. Xin, A. Manthiram, J. B. Goodenough, *J. Am. Chem. Soc.* **2016**, *138*, 9385–9388.
- [9] X.-B. Cheng, H.-J. Peng, J.-Q. Huang, R. Zhang, C.-Z. Zhao, Q. Zhang, *ACS Nano* **2015**, *9*, 6373–6382; H.-K. Kang, S.-G. Woo, J.-H. Kim, J.-S. Yu, S.-R. Lee, Y.-J. Kim, *ACS Appl. Mater. Interfaces* **2016**, *8*, 26895–26901; C. P. Yang, Y. X. Yin, S. F. Zhang, N. W. Li, Y. G. Guo, *Nat. Commun.* **2015**, *6*, 8058; Q. Yun, Y. B. He, W. Lv, Y. Zhao, B. Li, F. Kang, Q. H. Yang, *Adv. Mater.* **2016**, *28*, 6932–6939; Y. Sun, G. Zheng, Z. W. Seh, N. Liu, S. Wang, J. Sun, H. R. Lee, Y. Cui, *Chem* **2016**, *1*, 287–297; R. Zhang, N.-W. Li, X.-B. Cheng, Y.-X. Yin, Q. Zhang, Y.-G. Guo, *Adv. Sci.* **2017**, *4*, 1600445.
- [10] A. Pei, G. Zheng, F. Shi, Y. Li, Y. Cui, *Nano Lett.* **2017**, *17*, 1132–1139.
- [11] J. K. Stark, Y. Ding, P. A. Kohl, *J. Electrochem. Soc.* **2013**, *160*, D337–D342; K. N. Wood, E. Kazyak, A. F. Chadwick, K.-H. Chen, J.-G. Zhang, K. Thornton, N. P. Dasgupta, *ACS Cent. Sci.* **2016**, *2*, 790–801.
- [12] C.-M. Chen, Q. Zhang, X.-C. Zhao, B. Zhang, Q.-Q. Kong, M.-G. Yang, Q.-H. Yang, M.-Z. Wang, Y.-G. Yang, R. Schlogl, D. S. Su, *J. Mater. Chem.* **2012**, *22*, 14076–14084.
- [13] T.-Z. Hou, X. Chen, H.-J. Peng, J.-Q. Huang, B.-Q. Li, Q. Zhang, B. Li, *Small* **2016**, *12*, 3283–3291.
- [14] K. Yan, Z. Lu, H.-W. Lee, F. Xiong, P.-C. Hsu, Y. Li, J. Zhao, S. Chu, Y. Cui, *Nat. Energy* **2016**, *1*, 16010.
- [15] R. Mukherjee, A. V. Thomas, D. Datta, E. Singh, J. Li, O. Eksik, V. B. Shenoy, N. Koratkar, *Nat. Commun.* **2014**, *5*, 3710; R. Zhang, X.-B. Cheng, C.-Z. Zhao, H.-J. Peng, J.-L. Shi, J.-Q. Huang, J. Wang, F. Wei, Q. Zhang, *Adv. Mater.* **2016**, *28*, 2155–2162; K. Y. Xie, W. F. Wei, K. Yuan, W. Lu, M. Guo, Z. H. Li, Q. Song, X. R. Liu, J. G. Wang, C. Shen, *ACS Appl. Mater. Interfaces* **2016**, *8*, 26091–26097.

Manuscript received: February 26, 2017

Version of record online: May 3, 2017